3 Dynamics of Dislocations in a Two-dimensional System

K. Kaski, A. Kuronen, and M. Robles

Laboratory of Computational Engineering, Helsinki University of Technology P.O. Box 9400, FIN-02015 HUT, Finland.

Abstract. Dislocation dynamics in a two-dimensional Lennard-Jones solid is studied using an interactive simulation environment with on-line visualization. Movement of a dislocation in a homogeneous system under the influence of external stress and strain rate has been investigated. The results indicate that the simple model is capturing some essential characteristics of real materials. Investigation of strain relief in lattice-mismatched layer structures indicates that dislocation nucleation is asymmetric with respect to the sign of misfit. Moreover, dislocation reactions are observed that enhance the strain relief process.

3.1 Introduction

Dislocations play a central role in the theory of plasticity. Through their motion solids that display a ductile behaviour accommodate plastic deformation and thus avoid the catastrophic failure that is characteristic of brittle fracture. Therefore, the ease with which dislocations move in a solid, affects critically the behaviour of the solid under deformation. The dynamics of dislocations under different deformation processes has been the subject of a large number of both theoretical [1–3] and experimental [4–11] investigations.

The importance of the relation between dislocation velocity and externally applied stress has long been recognized. Four decades ago, in what possibly were the first experiments attempting to directly measure the velocity of dislocations, Johnston and Gilman [8] developed an experimental method which combined calibrated stress pulses with etch pitting technique. In their experiments dislocations were initially introduced by scratching the surface of a polished sample of known orientation. The position of some of the dislocations, prior and after the application of the pulse, were then determined through surface etching. Finally, the average velocity of the dislocations was estimated by dividing the measured distance between etch pits of the same dislocation by the time duration of the pulse. By varying the intensity of the pulse they were able to relate the measured velocity with the peak of the shear stress in the glide plane. Number of materials have been studied with this technique, first LiF, and then Ti [9], Cu [10], and $CuAl$ [11]. A further developed torsional stress pulse technique has been used in the study of dislocations in Cu, Zn and Al [12,13]. In most materials, experiments of this type yield a relation between dislocation velocity and shear stress in close

agreement with the power law

$$v = A\tau^m \,, \tag{3.1}$$

where A and m are material dependent constants. Small values of m are usually asociated with brittle materials while in a ductile material it may be very large.

The dislocation dynamics is also essential in strain relaxation processes of lattice-mismatched hetero-structures [14–16], central in todays nanotechnology. When in a lattice-mismatched hetero-structure the thickness of the overlayer is small enough, the mismatch is accommodated by elastic deformation of the overlayer. Such deformation keeps the overlayer in registry with the structure of the substrate crystal. When the thickness increases, the elastic energy of the overlayer becomes larger and at a certain critical thickness it becomes favorable to relieve the strain by misfit dislocations at the interface.

Various mechanisms of dislocation migration and nucleation have been found to affect the strain relaxation process [14,16]. These mechanisms include the migration of threading dislocation to the interface, nucleation of dislocations at overlayer surface or at island edges and dislocation multiplication [17–20]. In all these mechanisms the underlying atomic level cause of the misfit dislocation formation is the attractive force exerted by the interface on dislocations with Burgers vector orientation appropriate for the relaxation of misfit energy. Depending on the relative orientation of the interface with respect to the gliding planes and Burgers vectors of the affected dislocations, it could happen that the latter are not able to move to the interface. In this situation, if the misfit energy is high enough, dislocation reactions may take place prior to migration, with the re-orientation of the Burgers vectors of the migrating dislocations.

So far the modelling of strain relief mechanisms have in most cases been done within the framework of continuum elasticity theory. There are also some atomic level studies but they deal mostly with the static properties of misfit dislocations (see e.g. [21–25]). Furthermore, there are some studies on the dynamics or nucleation of dislocations [26–33], but to the best of our knowledge, no atomistic simulation studies on dislocation dynamics in the presence of a misfit interface in a hetero-structure has hitherto been carried out.

In the present work, we investigate the dynamics of dislocations in a two-dimensional (2D) solid using molecular dynamics (MD) simulations. In order to explore some qualitative features of dislocation dynamics and for simplicity, inter-atomic interactions have been modelled by Lennard-Jones (LJ) potentials. Sofar we have restricted our studies to 2D systems to avoid some of the geometrical complexities involved in simulating three-dimensional dislocations, while retaining some salient features of the problem under consideration. We will study the movement of dislocations in a homogeneous system under the influence of constant external stress and constant strain

rate. Moreover, the effect of the misfit interface on the nucleation and migration of dislocations will be investigated. By tuning the parameters of the potentials for the substrate and the overlayer we may construct a model of a hetero-interface with any desired value of lattice mismatch.

3.2   Dislocations in a 2D System

In this work, the interatomic interactions have been described with a Lennard-Jones pair potential, which means that the constructed lattice has to be close-packed, i.e. 2D hexagonal lattice. In this structure dislocations can be formed by removing one half of a row of densely packed atoms, which can be done in three orientations, as illustrated in Fig. 3.1a. This procedure introduces a partial dislocations and a stacking fault into the system (Fig. 3.1b). Such a configuration is unstable because a stacking fault in a 2D hexagonal lattice has a structure $ABAB|BABA$ with high potential energy. One should also note that due to high stacking fault energy dislocations in 2D systems do not dissociate into partials and a stacking fault ribbon as in 3D fcc lattice. By removing two half rows of atoms a stable (perfect) dislocation with a Burgers vector corresponding to the shortest lattice vector of the hexagonal structure is formed. An example of a stable dislocation with a Burgers vector $\mathbf{b} = [0\bar{1}]$ is shown Fig. 3.1c.

In the simulations pairs of dislocations were introduced into the system as a short and thin crack, see Fig. 3.2. On the other hand single dislocations can be introduced by making the crack so long that its other end is positioned outside the simulation system.
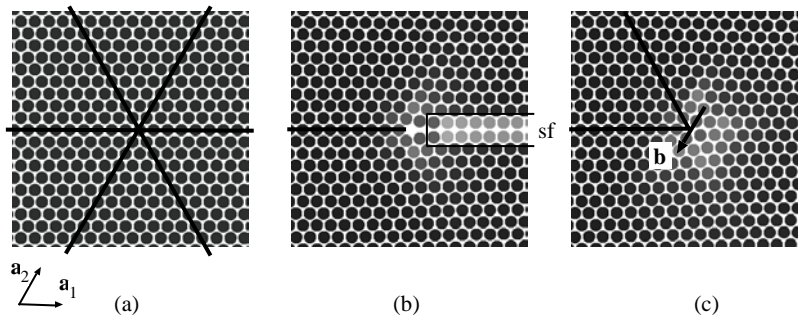
Fig. 3.1. Dislocations in the 2D hexagonal lattice. (**a**) Lattice contains three densely packed rows of atoms. Also shown are the lattice vectors $\mathbf{a}_1$ and $\mathbf{a}_2$ (magnified by 4 for better visibility). (**b**) Part of a dense row of atoms is removed for forming a partial dislocation and a stacking fault (sf). (**c**) By removing two dense rows a perfect dislocation is formed. Burgers vector of the dislocation $\mathbf{b}$ is magnified 4 times for better visibility. The shading of the atoms is coded according to their potential energy (light: high energy, dark: low energy)
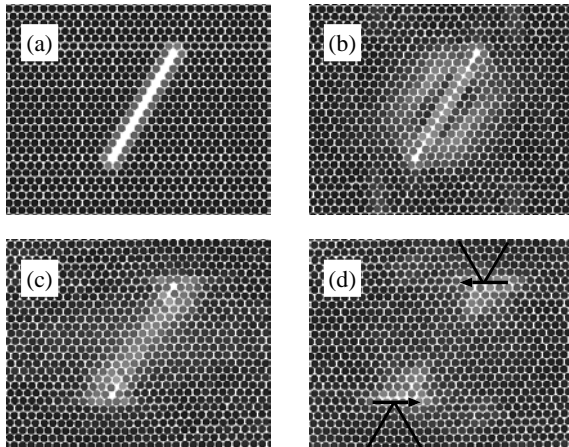
Fig. 3.2. Introduction of two perfect dislocations into the model system. (**a**) A part of a dense row of atoms is removed. (**b**) The vacancy loop collapses and forms two partial dislocations with a stacking fault between them. (**c,d**) The stacking fault heals by forming two perfect dislocations. The black lines denote the extra atomic rows forming the dislocations and arrows denote the Burgers vectors of the dislocations

3.3   Simulation Methods

3.3.1   Molecular Dynamics

In this study, the classical molecular dynamics (MD) simulation method is used, in which the interatomic interaction is described with the following Lennard-Jones pontential

$$V(r) = \epsilon_{\alpha\beta}[(\frac{\sigma_{\alpha\beta}}{r})^{12} - (\frac{\sigma_{\alpha\beta}}{r})^6]\,, \tag{3.2}$$

where r is the interatomic distance. Potential parameters $\epsilon_{\alpha\beta}$ and $\sigma_{\alpha\beta}$ depend on the species (α and β) of the interacting atoms. In the studies of dislocation dynamics under external force we have used homogeneous systems with only one type atomic species, i.e. $\epsilon_{\alpha\alpha} = \epsilon_{\beta\beta}$ and $\sigma_{\alpha\alpha} = \sigma_{\beta\beta}$. In the studies of the effect of misfit interface on dislocation we need to define the amount of lattice mismatch between the overlayer film and the substrate. This is done as follows

$$f = \frac{a_{\mathrm{f}} - a_{\mathrm{s}}}{a_{\mathrm{s}}}\,, \tag{3.3}$$

where a_{f} and a_{s} are the lattice constants in the film and the substrate, respectively. This mismatch can be incorporated into the simulations by assigning a different index for the atoms in the upper layers as compared to the atoms in the rest of the system and changing the equilibrium distance parameter

σ for these atoms accordingly. The cross-interactions between different types of atoms are calculated by the following interpolation scheme [34]:

$$\epsilon_{\alpha\beta} = \frac{2(\epsilon_{\alpha\alpha}\epsilon_{\beta\beta})^{1/2}\sigma_{\alpha\alpha}^3\sigma_{\beta\beta}^3}{\sigma_{\alpha\alpha}^6 + \sigma_{\beta\beta}^6} \tag{3.4}$$

$$\sigma_{\alpha\beta} = \left(\frac{\sigma_{\alpha\alpha}^6 + \sigma_{\beta\beta}^6}{2}\right)^{1/6}. \tag{3.5}$$

The values of parameters ϵ and σ, obtained by fitting to described copper [35], were used for the substrate atoms, though we emphasize that in this study our intention is not to describe any particular material. Instead our study is qualitative in nature. In the same spirit, the range of the potential is limited by the cut-off distance r_c chosen here to be $r_c = 2.1 \times r_{NN}$, where r_{NN} is the nearest neighbour distance. Since the discontinuity in the potential at the cut-off radius would cause a force anomaly, its effect is compensated by subtracting a linear term of the form $(r - r_c)dV/dr|_{r=r_c}$ from the potential.

In the calculation of pairwise interaction the standard MD method of linked lists was used [36]. The equations of motion were integrated by using the leap-frog form of the Verlet integration algorithm [36]. To achieve the desired temperature in the system both the simple velocity scaling and Berendsen scaling [37] were used. In cases where the atomic configuration with minimum potential energy was needed the following damping method was used:

$$\text{if } \mathbf{v}_i \cdot \mathbf{F}_i < 0 \text{ then } \mathbf{v}_i \leftarrow \alpha\mathbf{v}_i, \tag{3.6}$$

where $\mathbf{v}_i$ and $\mathbf{F}_i$ are the velocity and total force of atom i, respectively. A suitable value for the damping constant α (< 1) was found to be 0.9. This method was found to be more efficient in reaching equilibrium configuration in systems with a misfit interface than the normal cooling scheme.

3.3.2   Interactive Simulation Environment

In order to get better insight to the dislocation dynamics we have constructed a computational model that is based on an interactive simulation program with a graphical visualization environment, described in detail in [35]. Because of the exploratory nature of this work on-line visualization of simulation data is essential. The basic structure and an example of the main window of the simulation program are shown in Fig. 3.3.

This on-line visualization scheme makes it also possible to track various local defect configurations. For example when a 2D lattice is not externally deformed or is deformed only a little with a low strain rate, the potential energies of atoms show a clear change only near the core of a defect, i.e. of a dislocation or of a crack. Hence, it is possible to extract the subsets of atoms that belong to the defects of the system. Then by using a clustering algorithm the number of defects present in the system can be found. Following this, a
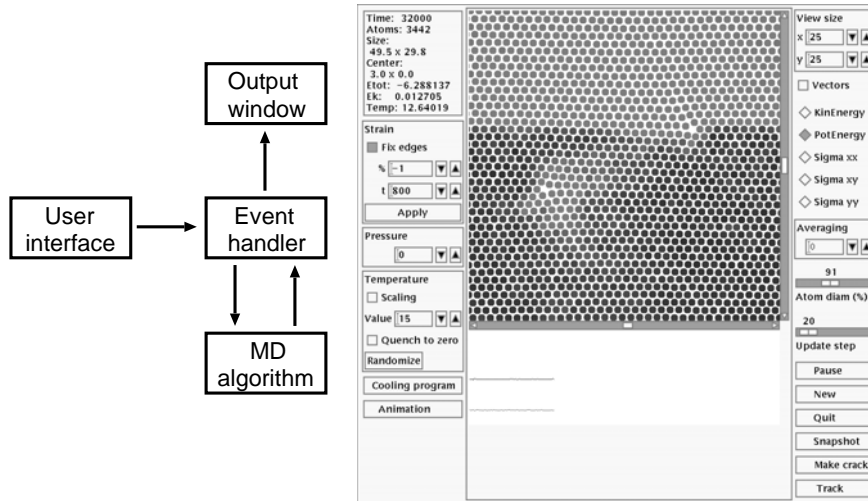
Fig. 3.3. The main window of the interactive simulation program. Positions of atoms are drawn in the center part of the window while various controls for changing simulation parameters are located on the edges of the window. Colors of the atoms can be used to display potential energy, kinetic energy or different components of the atomic level stress. On the left the main structure of the program is depicted

linked-list routine can be used to store efficiently the physical information of the constituent particles. In this way the position of center of mass, kinetic and potential energy, or even other geometrical properties, like the length of a crack or a dislocation can be extracted and followed. Moreover, it is possible to control the link-list routine during simulation through the control window where the main parameters of the clustering algorithm can be customized on-line. For the specific case of moving dislocations, the trajectory of the center of mass of the atoms in the core describes quite well its movement. A further analysis of the trajectories may be used to compute the instantaneous velocity of each dislocation, which is essential for the study of its dynamics.

3.4   Dynamics of Single Dislocation
in a Homogeneous System

In this section we describe an application of the interactive simulation enviroment to the study of the dynamics of a single dislocation moving in otherwise homogeneous lattice. The discussion concentrates on two aspects of the problem: (a) the interaction with external constant stress, and (b) the response to deformation with constant strain rate. Although these studies in 2D are exploratory in nature, they are hoped to shed some light to dislocation dynamics in a 3D system.

As mentioned above, by removing a portion of a line of atoms in the crystal and letting the system to relax it is possible to create a dislocation pair. By extending the removed line over the system border a single free dislocation is placed in the bulk material. By selecting the line properly, it is possible to introduce a dislocation at a desired position. All the experiments in this section were prepared by placing a single dislocation in the center of the sample. To guarantee that the dislocation is in a quasi-stable state, at least for the time scales used in the simulation, special care was taken in the selection of the sample size and in the choice of the thermal control for reduction of fluctuations as much as possible.

3.4.1   Constant Stress Deformation

In the first simulation experiment we applied a constant compressive displacement to the atoms of one of the side borders for a short period of time. Then if the opposite borders of the system are kept fixed – as done in this experiment – the system seems to stabilize rapidly to the condition of constant external force as shown in Fig. 3.4.

These simulation studies were carried out in a lattice of 22141 atoms arranged as a system of $L_x \times L_y = 120 \times 80$ (measured in terms of the lattice parameter a_0). The units used throughout this work are $a_0 = 3.6 \times 10^{-10}$ m, mass $m_0 = 1.055 \times 10^{-25}$ kg and time $t_0 = 10^{-12}$ s. No control of temperature was selected.

Figure 3.5 shows the characteristic displacement of the dislocation vs. time, for three force intensities. In each case a shock pulse is generated when one of the borders is rapidly moved. The dislocation initially wanders about its introduced position in a thermal-like motion until the pulse reaches it at $t \simeq 20$ ps. For small and moderate intensities of the external force, we observe three distinct phases in the dislocation motion. First, after being hit by the shock pulse the dislocation seems to be dragged by the stress wave and
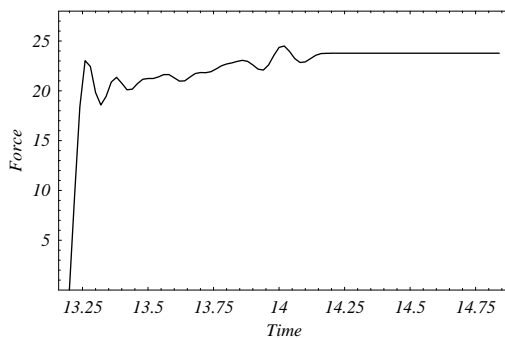
Fig. 3.4. External force profile after compressive displacement of the atoms of one of the side borders by 0.95% in 1 ps and thereafter keeping it and its opposite border fixed
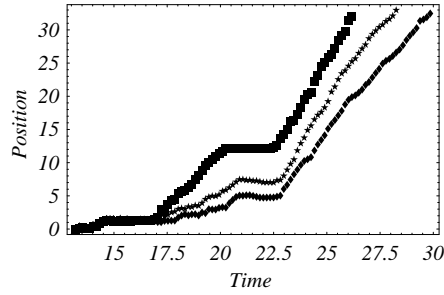
Fig. 3.5. Trajectory of one dislocation moving under constant stress at different stress values. The transient region (first and second phase) is due to interaction with the travelling shock wave
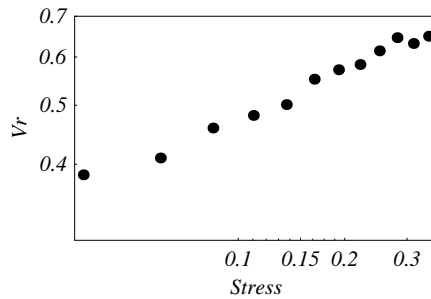
Fig. 3.6. Velocity (Vr) relative to the transverse speed of sound as a function of the external shear stress

travel along the glide line with a uniform velocity in the x-direction. Direct measurement of this dislocation velocity gives a value of about $14a_0/ps$, but its x-component is always smaller than the velocity of the propagating shock wave. The collision with the dislocation scatters the shock wave and thus begins a thermalization process. Few picoseconds later, in the second phase, the dislocation seems to be *released* from travelling with the wave and it stops moving. The displacement pattern in this phase resembles the motion seen before the interaction with the stress pulse.

Finally, in the third phase, the returning wave reflected from the opposite border hits the dislocation. Due to the enforced boundary condition on the y-borders, the reflected wave is also a compressive wave. As a result, the dislocation starts moving again with a uniform speed in the same direction as before, i.e. towards the upper border of the system. After this interaction the remaining diminished shock wave scatters once again to quickly thermalize the whole system to a new thermodynamic state. At this stage the dislocation seems to move under a constant shear stress and thermally stable condition. Therefore, we consider it possible to estimate the equilibrium velocity vs. stress relation, and the results are depicted in Fig. 3.6. Here the velocity has

been normalized by the transverse speed of sound estimated theoretically to be $8.34a_0/\text{ps}$.

The relation between stress and velocity seems to follow (3.1) with a sensitivity constant $m = 0.25$. This order of magnitude for the sensitivity constant is found experimentally for brittle materials indicating that the system studied here is capturing some properties of such materials. However, another possible explanation for this value is that the dislocation may be reaching a limiting velocity characteristic to the system, but due to the limitation of time and length scales of the simulations estimating the likelihood of this is beyond the scope of this study.

3.4.2 Constant Strain-Rate Deformation

In the second experiment the system is put under the influence of a constant strain-rate deformation, which is obtained by stretching the system from its y-borders in the x-direction with a constant velocity. The advantage of this set-up with respect to the constant force simulation is that it may be done in a quasi-static way to avoid generating shock waves.

In this case we chose again the hexagonal lattice with 38979 atoms arranged in a square of $130a_0$, and placing a single dislocation in the middle of the system. Here temperature control was applied by using Berendsen [37] thermostat at $3\,\text{K}$ to reduce the effect of phonons as much as possible. The stability of the dislocation turned out to be quite good for a time period of $20\,\text{ps}$, which is the duration of the whole experiment. The constant strain rate was realized by pulling the y-borders apart for $1-6\%$ of the system size in $20\,\text{ps}$.

When the deformation begins a potential energy wave is emitted from the borders. This causes, after some elapsed time, the dislocation movement. As this wave is an expansion wave (in contrast to the compressive wave in the constant stress experiment) the dislocation moves to the bottom of the sample, with a trajectory along the glide line, as depicted in Fig. 3.7a. From this curve we have computed the instantaneous velocity profile for the dislocation motion, with results shown in Fig. 3.7b.

The velocity profile is very characteristic to a rigid body movement in a continuous dissipative medium under the influence of a constant force. In this situation the equation of motion should have the form

$$m\dot{v} + Bv = f_e\,,\tag{3.7}$$

where v the instantaneous velocity, m the effective mass of the dislocation, B viscous drag coefficient and f_e the external source force. Solving this equation yields the following result

$$v = v_t(1 - e^{-t/t_0})\,.\tag{3.8}$$

where $v_t = f_e/B$ is the terminal velocity and $t_0 = m/B$ is the relaxation time for the dislocation motion. This behavior has been proposed to accurately
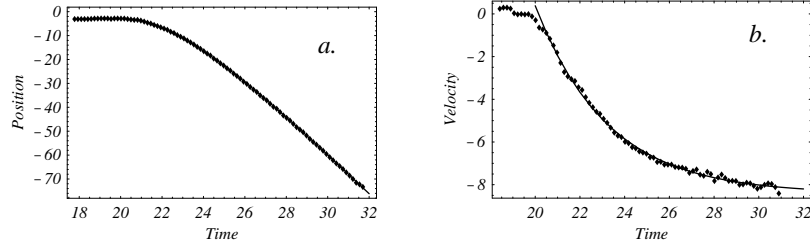
Fig. 3.7. (a) Trajectory of single dislocation moving along the glide line under a constant strain rate deformation (3% in 20 ps). (b) Instantaneous velocity for the data set in (a). The continuous line represents the best fit to the equation 3.8 of the velocity profile
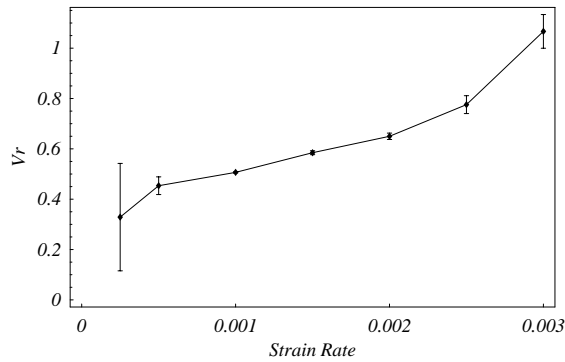
Fig. 3.8. Relative terminal velocity, $Vr = V/V_t$, for different strain rates (V_t stands for the transverse sound speed). The error bars were estimated by randomizing the initial state with different random number seeds

describe dislocation movement in metals [12], when the external force is given in terms the resolved shear stress and the magnitude of the Burgers vector, as $f_e = b\tau$.

From the simulations we found, as expected, that the time variation of the external force is compatible with the type II elastic – homogeneous plastic response [38], showing strain-hardening coefficient dependent on the strain rate. This coefficient is found to take value of 1.0 (Hooke's law) for low strain rates to decrease to 0.45 (characteristic for metals) for highest strain rates.

Although the external force (and hence the true stress) is known, the resolved shear stress affecting the dislocation is unclear, and its determination is not simple. One possibility to determine it is trying to map the dislocation trajectories to some constant stress experiments, done with the same simulation parameters and assuming that the causes of the dislocation movement are the same in both cases. This may be done through the strain-rate–velocity (see Fig. 3.8) and stress–velocity relations. Such study is still under development.

3.5   Interaction Between Dislocations and a Misfit Interface

In the studies described above the stress affecting dislocation movement was external. In lattice-mismatched structures the stress comes from the misfit interface. In the following we describe simulation studies of the strain relief process in a lattice-mismatched system via dislocation nucleation and dislocation reactions and subsequent migration to the interface.

3.5.1   Dislocation Nucleation

Nucleation simulations were performed using a system consisting of a substrate of size $722\,\text{Å} \times 361\,\text{Å}$. The overlayer placed on the substrate had a size of $361\,\text{Å} \times 361\,\text{Å}$, i.e. half of the width of the substrate. The total number of substrate and overlayer atoms was 23076 and 11590, respectively.

Simulations were performed for misfits -2.0–-4.0% and $+2.0$–$+4.0\%$ at temperatures 10–160 K. The initial states of the simulations were obtained by applying the quenching method of 3.6. The simulation time was 130 ps. Results are shown in Fig. 3.9. In the region of low misfit and low temperature no dislocations were seen. In this region, the strain was relieved by elastic deformation of the overlayer and substrate. By increasing the temperature dislocations were seen to nucleate from the overlayer edges. In all other cases except the -2.0%, $+2.0\%$, and $+2.5\%$ misfits the highest temperature of 160 K was enough to reach the equilibrium configuration (number of dislocations of 4, 4, 3, 2, and 1 for the misfits $\pm 4.0\%$, $\pm 3.5\%$, $\pm 3.0\%$, $\pm 2.5\%$, and $\pm 2.0\%$, respectively). In the case of misfit of $\pm 4.0\%$, dislocations were observed even in simulations with zero initial temperature, indicating that
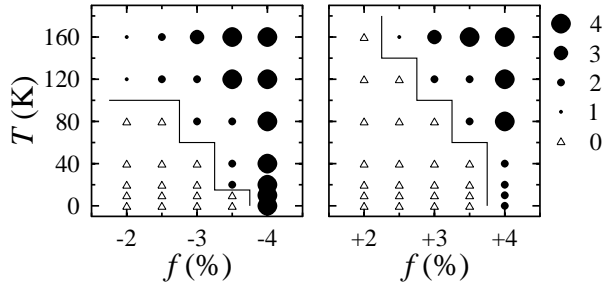
Fig. 3.9. Results of nucleation simulations. The number of dislocations nucleated from the overlayer edges during the 130 ps simulations is plotted for different negative (left) and positive (right) misfit values and simulation temperatures. The size of the circles denotes the number of dislocations. Open triangles designate runs where no dislocations were observed. The thin line separates pseudomorphic and relaxed regions

the activation barrier for nucleation disappears. The results also show that the situation is not symmetric with respect to changing the sign of the misfit: negative misfit is considerably more efficient in causing dislocation nucleation on the overlayer edges. One possible explanation is that strain caused by the negative mismatch lowers the dislocation nucleation barrier by pulling the overlayer corners away from the substrate surface. This same asymmetry has been observed in dislocation nucleation from the overlayer surface [30].

3.5.2   Dislocation Reactions

In the simulations described below we studied a system, which in most cases consisted of 30 rows of substrate atoms and 19 rows of overlayer atoms, in total 3442 atoms. The bottom layer of the substrate atoms is fixed in the vertical direction while the other boundaries of the system are free to move in any direction. We also investigated the effect of system size by performing simulation runs with a four times larger system (of 13712 atoms) where the width and the height of the system were doubled but the overlayer thickness
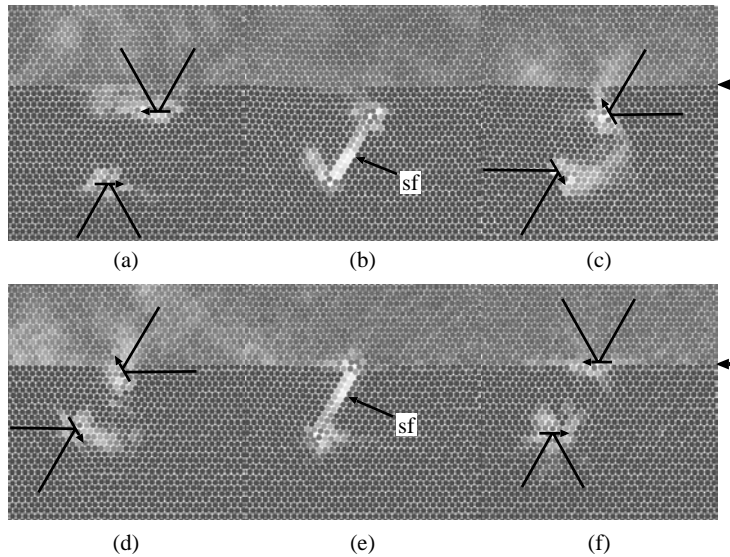
Fig. 3.10. Reaction between dislocations and the misfit interface. The lattice mismatch between the overlayer and the substrate is $f = -4\%$ (**a**) [Elapsed time from the beginning of the simulation $t = 12.1\,\text{ps}$] Two dislocations with horizontal Burgers vectors are introduced to the system. (**b,c**) [$t = 15.1, 16.1\,\text{ps}$] These interact with each other forming first a stacking fault (sf) between them and then dislocations with Burgers vectors oriented $60°$ relative to the x-axis. (**d**) [$t = 18.8\,\text{ps}$] The upper dislocation migrates to the interface. (**e,f**) [$t = 33.5, 34.2\,\text{ps}$] The dislocations interact once again and turn their Burgers vectors horizontally. The small arrows show the position of the interface

was kept the same as in the smaller system. In this case we saw similar dislocation reactions as in the smaller system but with a slightly different set of simulation parameters, thus indicating that although the details of dislocation dynamics may depend on the system size the reaction behaviour remains unchanged.

Figure 3.10 depicts an example of the effect of an interface on dislocations, when the lattice mismatch is set $f = -4\%$. In order to introduce a pair of dislocations into the system a short initial crack was introduced first. Then the system was let to heal for 10 ps during which the temperature was scaled to 15 K at every time step followed by switching off the scaling and letting the simulation continue by keeping the total energy constant. The upper dislocation – having two extra planes in the positive y-direction – has the maximum capability to relieve stress formed at the interface (see Fig. 3.10a). However, this dislocation cannot glide to the interface because its Burgers vector is horizontal.

Figure 3.10b shows how the interaction between the dislocations induces a reaction that results in changes in their Burgers vectors. The fact that the sum of Burgers vector does not change in this reaction can be easily verified. After the reaction the upper dislocation is able to glide to the interface. However, its Burgers vector is not ideal in relieving stress at the interface. In Fig. 3.10d–e a further reaction can be seen which gives rise to dislocations with horizontal Burgers vectors (Fig. 3.10f). The upper dislocation is now located at the interface and it has the optimum orientation – i.e. parallel to the interface – as regards to the stress relief. The lower dislocation finally glides to the free boundary of the system, where a step is created. Reactions between dislocations proceed through creation of two partial dislocations and a stacking fault between them, and thus a slip of two adjacent atomic rows
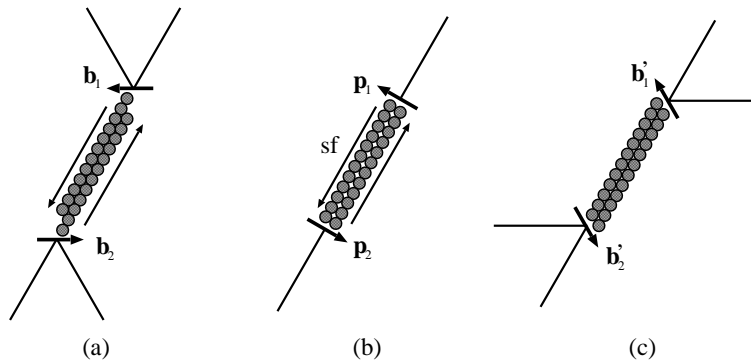
Fig. 3.11. Two dislocations before (**a**) and after (**c**) the reaction depicted in Fig. 3.10a–c. The reaction proceeds through a configuration with two partial dislocations ($\mathbf{p}_1$ and $\mathbf{p}_2$) and a stacking fault (sf) between them. The slip of two atom rows between the dislocation cores causes the Burgers vectors of the dislocation to turn 60° clockwise. Thin lines show the orientation of extra half rows of atoms

with respect to each other, as can be seen in Fig. 3.11. The reaction could also be viewed as an exchange of one complete dislocation between the participating dislocations. However, because the distance between the dislocations is so small this third dislocation can not be distinguished. For the reaction to take place the dislocation cores have to lie at the same densely packed row of atoms. Similar reactions were also observed in the cases where the mismatch was positive, i.e. $f = +4\%$.

3.6   Conclusions

The main goal of these exploratory studies has been to use a simplistic model that may be analyzed interactively and captures essential information about dislocation dynamics in homogeneous and strained-layer systems. The questions of the resolved shear stress in the constant strain rate experiments and the presence of a dislocation dragging are beyond the possiblities of the continuum theory. Also, the strain relief in lattice-mismatched systems via dislocation nucleation, migration and interaction are hard to study in detail using continuum theories. Simple atomic scale simulations may give more information for new theoretical approaches and modelling.

References

1. A.J.E. Foreman and M.J. Makin: Phil. Mag. **14**, 911 (1960)
2. A.S. Krausz: Mat. Sci. Eng. **6**, 260 (1970)
3. T. Munakata and A. Igarashi: Phys.Rev. B. **46**, 13786 (1992)
4. J.J. Gilman and W.G. Johnston: J. Appl. Phys. **31**, 687 (1960)
5. D.F. Stein and J.R. Low Jr.: J. Appl. Phys. **31**, 362 (1960)
6. H. Ney, R. Labusch and P. Haasen: Acta Metall. **25**, 1257 (1977)
7. C.S. Pang and J.M. Galligan: Phys. Rev. Lett. **43**, 1595 (1979)
8. W.G. Johnston and J. Gilman: J. Appl. Phys. **30**, 129 (1959)
9. T. Tanaka and H. Conrad: Acta Metall. **19**, 1001 (1971)
10. W.F. Greenman, T. Vreeland, and D.S. Wood:
11. M. Kleintges, R. Labusch, H.G. Brion, and P. Haasen: Acta Metall. **25**, 1247 (1977)
12. K.M. Jassby and T. Vreeland Jr.: Phil Mag. **21**, 1147 (1970)
13. T. Vreeland Jr. and K.M. Jassby: Mater. Sci. Eng. **7**, 95 (1971)
14. E.A. Fitzgerald: Mat. Sci. Rep. **7** 87–142 (1991)
15. R. Hull and J.C. Bean: Crit. Rev. Solid State. Mat. Sci. **17**, 507–546 (1992)
16. R. Hull and E.A. Stach: In: *Thin Films: Heteroepitaxial Systems,* ed. by A.W.K. Liu and M.B. Santos. (Series on Directions in Condensed Matter Physics, vol.15) (World Scientific, Singapore 1999) pp. 299–367
17. J.W. Matthews: J. Vac. Sci. Technol. **12**, 126–133 (1975) (See also [14] for a discussion of the work by Matthews et al.)
18. H. Strunk, W. Hagen, and E. Bauser: Appl. Phys. **18**, 67–75 (1979)
19. W. Hagen and H. Strunk: Appl. Phys. **17**, 85–87 (1978)

20. F.K. LeGoues, B.S. Meyerson and J.F. Morar: Phys. Rev. Lett. **66**, 2903–2906 (1991)
21. P. Ashu and C.C. Matthai: Appl. Surf. Sci. **48/49**, 39–43 (1991)
22. P. Gumbsch, M.S. Daw, S.M. Foiles, and H.F. Fischmeister: Phys. Rev. B **43**, 13833–13837 (1991)
23. L.A. Zepeda-Ruiz, D. Maroudas, and W.H. Weinberg: Surf. Sci. **418**, L68–L72 (1998)
24. M. Dornheim and H. Teichler: Phys. Stat. Sol. **A171**, 267–274 (1999)
25. P.A. Ashu, J.H. Jefferson, A.G. Cullis, W.E. Hagston, and C.R. Whitehouse: J. Crystal Growth **150**, 176–179 (1996)
26. G.J. Dienes, K. Sieradzki, A. Paskin, and B. Massoumzadeh: Surf. Sci. **144**, 273–289 (1984)
27. L. Dong, J. Schnitker, R.W. Smith, and D.J. Srolovitz: J. Appl. Phys. **83**, 217–227 (1998)
28. S. Swaminarayan, R. LeSar, P. Lomdahl, and D. Beazley:
29. H. Gao, C.S. Ozkan, W.D. Nix, J.A. Zimmerman, and L.B. Freund: Phil. Mag. A **79**, 349–370 (1999)
30. S. Brochard, P. Beauchamp, and J. Grilhé: Phil. Mag. A **80**, 503–524 (2000)
31. A. Aslanides and V. Pontikis: Phil. Mag. A **80**, 2337–2353 (2000)
32. M.E. Bachlechner, A. Omeltchenko, A. Nakano, R.K. Kalia, P. Vashishta, I. Ebbsjö, and A. Madhukar: Phys. Rev. Lett. **84**, 322–325 (2000)
33. B. Joós, Q. Ren, M.S. Duesbury: Surf. Sci. **302**, 385–394 (1994)
34. M. Diaz Peña, C. Pando, and J.A.R. Renuncio: J. Chem. Phys. **76**, 325–332 (1982)
35. J. Merimaa, L.F. Perondi, and K. Kaski: Comp. Phys. Comm. **124**, 60 (1999)
36. M.P. Allen and D.J. Tildesley: *Computer Simulation of Liquids.* (Clarendon Press, Oxford 1987)
37. H.J.C. Berendsen, J.P.M. Postma, W.F. van Gunsteren, A. DiNiola, and J. R. Haak: J. Chem. Phys. **81**, 3684–3690 (1984)
38. R.W. Hertzberg: *Deformation and Fracture Mechanics of Engineering Materials.* 4th edn. (John Wiley, USA 1996)